Carbon Letters (2024) 34:13–24
https://doi.org/10.1007/s42823-023-00608-x

Online ISSN 2233-4998
Print ISSN 1976-4251

ORIGINAL ARTICLE

Structural, optical and photovoltaic properties of V_2O_5/ZnO and reduced graphene oxide (rGO)-V_2O_5/ZnO nanocomposite photoanodes for dye-sensitized solar cells

C. Bhagya Lakshmi[1] · S. Anna Venus[1] · S. Velanganni[2] · A. Muthukrishnaraj[3] · Manikandan Ayyar[4,5,6] · Mohamed Henini[7,8,9]

Received: 3 July 2023 / Revised: 12 August 2023 / Accepted: 3 September 2023 / Published online: 14 September 2023

Abstract

Photoanode optimization is a fascinating technique for enlightening the power conversion efficiency (PCE) of dye-sensitized solar cells (DSSCs). In this present study, V_2O_5/ZnO and reduced graphene oxide (rGO)-V_2O_5/ZnO nanocomposites (NCs) were prepared by the solid-state technique and used as photoanodes for DSSCs. A wet chemical technique was implemented to generate individual V_2O_5 and ZnO nanoparticles (NPs). The structural characteristics of the as-synthesized NCs were investigated and confirmed using powder X-ray diffraction (XRD), X-ray photoelectron spectra (XPS), and Scanning electron microscope (SEM) with energy dispersive X-ray (EDX) analysis. The average crystallite size (D) of the as-synthesized V_2O_5/ZnO and rGO-V_2O_5/ZnO NCs was determined by Debye-Scherer's formula. The bandgap (eV) energy was calculated from Tauc's plots, and the bonding nature and detection of the excitation of electrons were investigated using the Ultra violet (UV) visible spectra, Fourier Transform infrared (FTIR) and photoluminescence (PL) spectral analysis. Electrical studies like Hall effect analysis and the Nyquist plots are also described. The V_2O_5/ZnO and rGO-V_2O_5/ZnO NCs based DSSCs exhibited 0.64% and 1.27% of PCE and the short circuit current densities and open circuit voltages improved from 7.10 to 11.28 mA/cm^2 and from 0.57 to 0.68 V, respectively.

Keywords ZnO · Nanocomposites · Graphene oxide · XPS spectrum · Dye-sensitized solar cells

✉ C. Bhagya Lakshmi
bhagya.jey@gmail.com

✉ S. Anna Venus
annavenus@stxavierstn.edu.in

✉ Manikandan Ayyar
manikandan.frsc@gmail.com

[1] Department of Physics, Energy Research Centre, St. Xavier's College (Autonomous) affiliated to Manonmanium Sundaranar University, Palayamkottai, Tirunelveli 627002, India

[2] Department of Chemistry, Parvathy's Arts and Science College (affiliated to Madurai Kamaraj University), Dindigul 624002, India

[3] Department of Chemistry, Faculty of Engineering, Karpagam Academy of Higher Education, Coimbatore, Tamil Nadu 641021, India

[4] Department of Chemistry, Karpagam Academy of Higher Education, Coimbatore, Tamil Nadu 641021, India

[5] Centre for Material Chemistry, Karpagam Academy of Higher Education, Coimbatore, Tamil Nadu 641021, India

[6] Department of Chemistry, Bharath Institute of Higher Education and Research (BIHER), Chennai 600073, Tamil Nadu, India

[7] UNESCO UNISA Africa Chair in Nanosciences and Nanotechnology, College of Graduate Studies, University of South Africa, Muckleneuk Ridge, PO Box 392, Pretoria, South Africa

[8] Nanosciences African Network (NANO-AFNET), iThemba LABS-National Research Foundation, 1 Old Faure Road, Somerset West, PO Box: 722, Cape Town 7129, South Africa

[9] School of Physics and Astronomy, University of Nottingham, Nottingham NG7 2RD, UK

1 Introduction

Recently, dye-sensitized solar cells (DSSCs) can be seen as a talented alternate to the conservative photovoltaic strategies and has fascinated significant consideration as they offer the opportunity for low-cost and also high alteration photovoltaic (PV) energy [1–3]. Over the last decade, researchers have concentrated on developing a photoanode (working electrode) with a diversity of morphologies in order to expand the proficiency of DSSCs. TiO_2 is the greatest often active photoanode substantial in DSSCs, owing to its porosity and durable catalytic nature. Recently discovered interface properties such as charge departure, converse recombination, and tricking of photogenerated electrons in semiconductor device outsides self-sufficiently by defining optimal material mixtures and their gathering [4, 5]. To maximize overall energy conversion efficiency (ECE), it is essential to construct a combination of materials consisting of various metal oxide semiconductors (MOS) that reduces recombination currents, improves light absorption, ensures a good electric connection.

Since of their low cost, eco-friendly stewardship, and significant production, carbonous materials are widely working to progress photocatalytic (PC) and photovoltaic (PV) activities. Recently, reduced graphene oxide (rGO) has been extensively employed as an active subsidiary material for attractive charge transfer and adsorption capacities owing to its exceptional attributes such as superior electrical conductivity (EC), high surface area and also good optical properties. Additionally, the combination of rGO with metal oxides can provide numerous advantages, including increased performance rate, longer cyclability, and higher sulphur consumption rates [6, 7]. Metal oxide/rGO NCs are believed to be an important approach towards broadening the possibilities of MOS in fields such as energy gathering, alteration, and loading devices. Various kinds of MOS including rGO-TiO_2, rGO-V_2O_5, rGO-ZnO, rGO-SnO_2, and rGO-Nb_2O_5, etc. have been reported [8].

The various V_2O_5 based attached semiconductors, including V_2O_5/$BiVO_4$, V_2O_5/SiO_2, TiO_2/V_2O_5, V_2O_5/ZnO Au/V_2O_5/ZnO, Ag_2O/V_2O_5/TiO_2, RGO/V_2O_5 and carbon nanostructures/V_2O_5, have been successfully synthesized in recent years [9–16]. Recently, Saravanan et al. reported photocatalytic (PCD) property of V_2O_5/ZnO NCs synthesized by hydrothermal route [12]. Yin et al. reported the synthesis and plasmonic PCD activity of Au-decorated V_2O_5@ZnO materials [13]. Boruah et al. studied the Fe_3O_4@V_2O_5/rGO NCs as environmental photocatalyst [15].

In this perspective, it is desirable to study the photovoltaic (PV) behavior of rGO-V_2O_5/ZnO NCs. Herein, for the first time we introduce the synthesis of V_2O_5 /ZnO and rGO-V_2O_5/ZnO NCs as photoanode material and fabricated a DSSC cell. Therefore, rGO-V_2O_5/ZnO NCs may provide a new generation of materials for outstanding PV activity [16–20]. In the current study, we describe the solid-state reaction mixture method used to synthesize V_2O_5/ZnO and rGO-V_2O_5 /ZnO NCs. We have investigated physical and chemical properties using XRD, SEM with EDX, XPS, UV–Vis, FT-IR, PL spectra, Hall effect and impedance analysis. The photovoltaic (PV) performance of V_2O_5 /ZnO and rGO-V_2O_5/ZnO NCs integrated photoanode in DSSCs was assessed under ordinary simulated sun light intensity of 100 mW cm^{-2}.

2 Experimental details

2.1 Materials

As precursors, cetyl trimethyl ammonium bromide (CTAB), sodium metavanadate, ammonium chloride (NH_4Cl), zinc nitrate, sodium hydroxide, rGO and ethanol solution are employed. The materials are purchased in Hi-media AR grade used without additional purification. Pilkington provided indium doped tin oxide glass plates (TEC7) with resistance of 15–25 Ω/cm^{-2}. N719 dye was acquired from Sigma-Aldrich. For sample preparation and washings, double deionised (DD) water was used.

2.2 Characterization techniques

Crystalline structure of V_2O_5 /ZnO and rGO-V_2O_5/ZnO NCs were characterized by PAN analytical X'PERT PRO diffractometer (Cu Ka radiation, $k = 1.54$ Å). Scanning electron microscopy (JEOL-JSM 5610LV) coupled with an energy-dispersive X ray (EDX) analyser was used to investigate the morphology and elemental compositions of the as-prepared composites. The ULVAC-PHI X-Ray photoelectron spectrometer was employed for XPS analysis (PHI5000). The FTIR spectrum was obtained using a Perkin Elmer Spectrum Two instrument with a range of 4000–400 cm^{-1}. Shimadzu model spectrometer was used to record the UV–Visible spectrum. The PL spectrum was measured with a Shimadzu RF-5301PC spectro-fluorophotometer. Ecopia HMS-7000 Photonic Hall Effect Measurement System was used to determine electrical properties such as carrier concentration (n), mobility (μ), resistivity (ρ) and conductivity (σ). Hioki IM3536 General Purpose LCR Meter, DC 4 Hz to 8 MHz, was used to measure the impedance [ratio of Voltage to Current (V/I)] value. Photo Emission Technology solar simulator from Newport (Oriel QEPVSI-B IPCE System) was used for current–voltage characterization studies.

2.3 Synthesis of V_2O_5 and ZnO nanoparticles

The synthesis of vanadium penta oxide (V_2O_5) and zinc oxide (ZnO) nanoparticles (NPs) were prepared by chemical wet method. Initially, 100 ml of DD water with 8 mM sodium metavanadate fully dissolved was subjected to continual stirring. After that, the solution was thoroughly dissolved in 200 mM of NH_4Cl. After a few minutes, the solution's colour changed from murky to clear, then to smokey. Ten minutes later, 10 mM of Cetyl trimethyl ammonium bromide (CTAB) was included in the solution, and the temperature of the synthesis was elevated to 80 °C. Colour of the solution transformed from orange to dark brown. A transparent yellow colour appeared in the solution after an hour. The final product was dried for 4 h, then permitted to cool to ambient temperature and calcinated for 4 h at 420 °C.

For preparation of ZnO NPs, 1.2 M of sodium hydroxide (NaOH) in aqueous ethanol solution and 0.7 M of zinc nitrate in aqueous ethanol solution were both stirred for an hour. The prepared NaOH aqueous solution was added dropwise to the zinc nitrate solution while being constantly stirred at high speed. The remaining sodium hydroxide was added, and the reaction was allowed to proceed for 2 h. After being centrifuged for 10 min at 6000 rpm, the solution was left to settle for a few hours. Thus, precipitated ZnO NPs were dried in a muffle furnace for 1 h at 60 °C and the final product was then annealed at a temperature of 420 °C.

2.4 Synthesis of rGO-V_2O_5/ZnO nanocomposites

The process of rGO-V_2O_5/ZnO NCs was carried out via standard solid-state reaction method. Prepared V_2O_5 and ZnO NPs were mixed with rGO in various stochiometric ratios. The mixture was extensively crushed in a mortar and pestle to obtain the best reaction activity and homogeneity. Ethanol was slightly added as a solvent to serve as a reaction medium. The combined mixture was heated at 450 °C for 6 h in a muffle furnace and was eventually cooled to room temperature before being taken out. A schematic diagram of solid-state reaction method for the preparation is shown in Fig. 1.

2.5 Fabrication of photoanodes

The ITO glasses were cleaned in an ultrasonic water bath with acetone, ethanol, and DD water before being dried in hot air. The doctor blade technique was implemented to coat a photoanode consisting of prepared NCs (V_2O_5/ZnO and rGO-V_2O_5/ZnO). Before starting the slurry coating procedure, the necessary amount of rGO-V_2O_5/ZnO NCs powder and acetyl acetone is coarsely crushed in a mortar. ITO slides were coated with a fine slurry of rGO-V_2O_5/ZnO and dried in a muffle furnace for 30 min at 420 °C. The consistent approach was employed to generate the V_2O_5/ZnO photoanodes. Dropping chloroplatanic hydrate acid on a conducting glass substrate and annealing it in air at 420 °C for 30 min resulted in the formation of a Pt electrode [21, 22]. Figure 2 shows coated photoanodes made from V_2O_5/ZnO and rGO-V_2O_5/ZnO NCs.

2.6 Fabrication of DSSCs

In general, the produced photoanodes were immersed in a solution containing N719 dye for 24 h in a dark environment

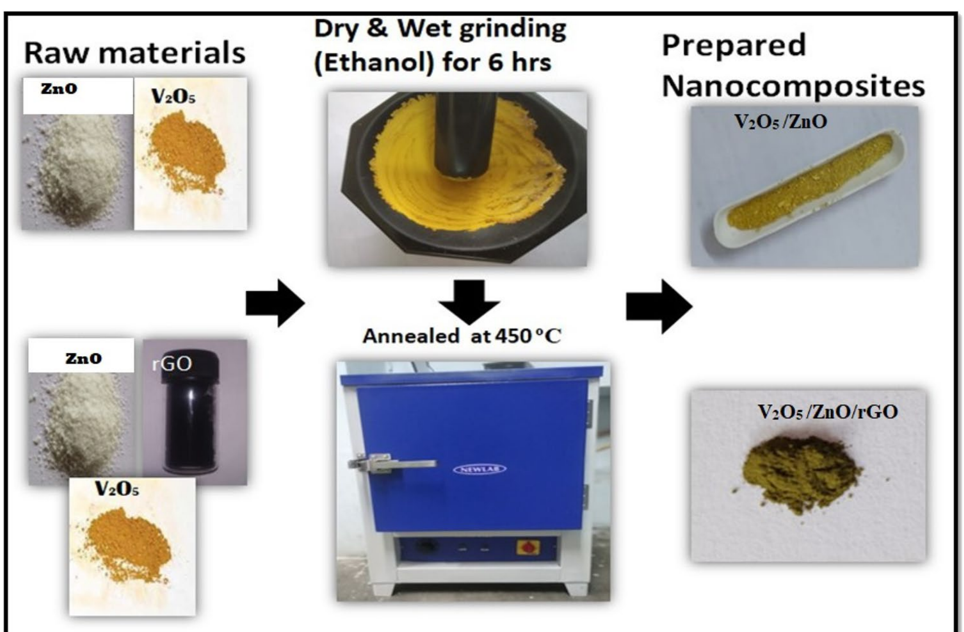

Fig. 1 Schematic diagram of synthesis of nanocomposites

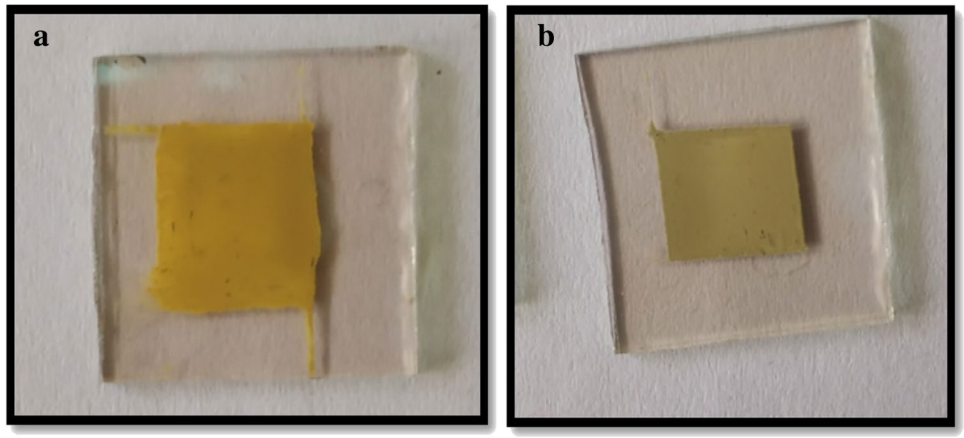

Fig. 2 Prepared V_2O_5/ZnO and rGO-V_2O_5/ZnO photoanodes

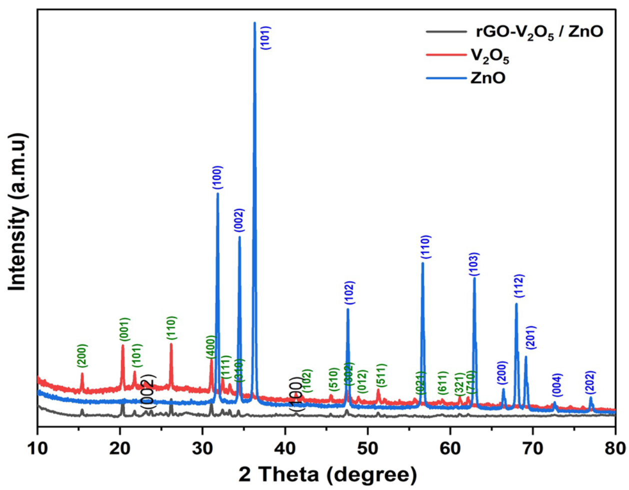

Fig. 3 XRD pattern of V_2O_5, ZnO and rGO-V_2O_5/ZnO NCs

[23]. Following the dye adsorption, the substrates were rinsed with ethanol to remove excess dye and dried in hot air. Consequently, the DSSCs were fabricated by clipping together prepared photoanodes with Pt counter electrodes. The I-/I_3- redox electrolyte, which included NaI and I_2, was injected into the DSSCs using a small syringe [24]. The calculated active regions of cells are 1.1 cm^2. All the fabrication and characterization processes were carried out in an ambient atmosphere without any protective atmosphere.

3 Results and discussions

3.1 XRD diffraction analysis

Figure 3 shows the XRD pattern of as-synthesised V_2O_5, ZnO NPs and rGO-V_2O_5/ZnO NCs. The V_2O_5 individual peaks have 2θ values at 15.23°, 20.66°, 25.91°, 29.16°, 37.43°, 40.59°, 43.12°, 44.19°, 45.53°, 46.10°, 49.20°, 51.73° and 57.3° equivalent to the planes (200), (001), (110), (301), (407), (311), (102), (202), (411), (510), (112), (212) and (121), respectively. This result reveals that V_2O_5 phase (orthorhombic) is well aligned with standard data base of JCPDS card no: 77-2418. On the other hand, the observed 2θ peaks for ZnO of 32.29°, 34.89°, 36.74°, 47.93°, 63.25°, 66.84°, 68.37° and 69.52° correspond to (100), (002), (101), (102), (103), (200), (112) and (201) planes, respectively, and are matched with JCPDS card no 89-1397. The minor detected peaks at 22.08° and 41.98° are related to the (002) and (100) plane of rGO, respectively. Similar results were reported by Stobinski et al. [25]. The calculated average crystallite size (D) of the rGO-V_2O_5/ZnO is found to be 14.12 nm using Debye Scherrer's formula.

3.2 SEM with EDX analysis

The surface morphology and average particle size was examined by scanning electron microscopy (SEM) analysis (Fig. 4). V_2O_5/ZnO possess a cluster of spherical shaped materials with particle size of ~ 36.8 nm (Fig. 4a, b) and it is also evident that there are very tiny group of small clusters stacked together with diameter of 13 to 25 nm spheres in the case of V_2O_5/ZnO/rGO (Fig. 4c, d), which indicates the presence of rGO in the NCs. It is important to note that the average crystallite sizes results obtained from XRD are well matched with SEM images. From EDX analysis, it is confirmed that the as-prepared samples have no impurities and have 50.92% of C, 22.65% of O, 17.37% of V and 9.06% of Zn for V_2O_5/ZnO/rGO NCs and for 24.45% of O, 51.87% of V and 23.67% of Zn for V_2O_5/ZnO (Fig. 5) [26].

3.3 XPS spectrum

To probe the electronic structure and chemical environment, XPS spectra are investigated. All four elements (C, V, O and Zn) given by XPS scan are shown in Fig. 6a. The XPS spectrum for rGO—V_2O_5/ZnO NCs indicate the presence of C 1 s at 284.8–289.1 eV, V 2p at 517–535 eV, O 1 s at

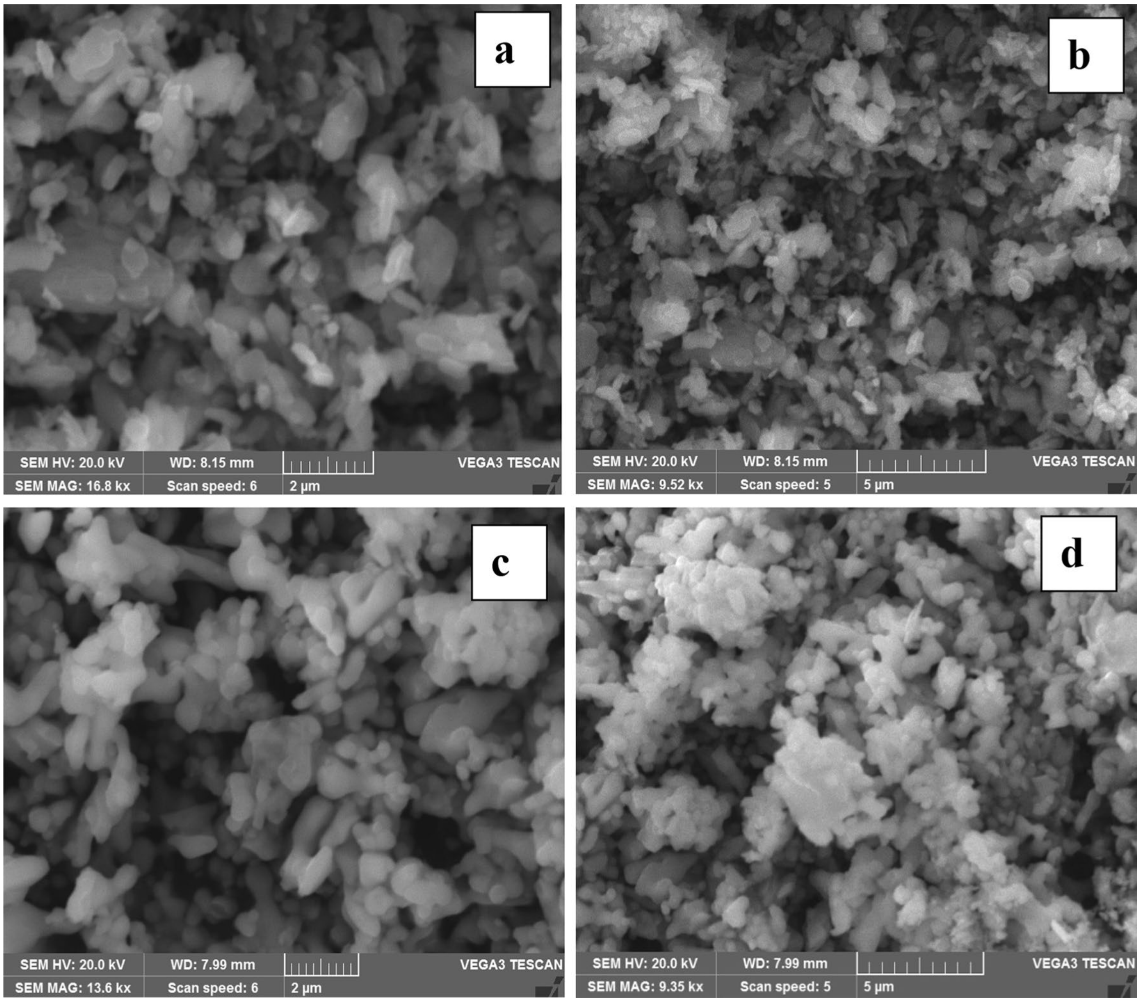

Fig. 4 SEM Images of **a**, **b** 2 µm, 5 µm for V_2O_5/ZnO and **c**, **d** 2 µm, 5 µm for rGO-V_2O_5/ZnO nanocomposites

530.5–532.5 eV, and Zn 2p at 497 eV-1021 eV as illustrated in Fig. 6a.

The XPS scan for carbon content in the samples confirms the C 1 s peaks (Fig. 6b) at 284.8 eV, 286 eV and 289.1 eV. Furthermore, the XPS scan for vanadium shows peaks at 517.7 eV and 525 eV ascribed to V $2p_{3/2}$ and V $2p_{1/2}$, respectively. The small minor peaks at 530.5 eV and 532.4 eV of V 2p peaks confirm the presence of vanadium (Fig. 6c). In Zn 2p spectrum (Fig. 6d), Zn $2p_{3/2}$ peak is observed at a binding energy of 1021.6 eV indicating the presence of Zn content. As shown in Fig. 6e, the high intensity peaks at 530.5 eV and 532.4 eV are attributed to O 1 s [27–29] and confirm the presence of oxygen.

3.4 UV ViS analysis

The prepared rGO-V_2O_5 /ZnO NCs have absorption in the visible and UV range of the light spectrum with an absorption edge at 582 nm, whereas the V_2O_5/ZnO NCs have UV light absorption edge between ~ 320 and 585 nm. From Fig. 7a, it is noticeable that absorption bands move towards the lower wavelength (blue shift) compared to rGO-V_2O_5/ZnO NCs. To find the conducting behavior, we have determined the bandgap energy (*Eg*) of synthesized NCs. The *Eg* values, which were calculated by plotting Taucs plot graphs, are found to be 2.54 eV for V_2O_5/ZnO and 2.64 eV for rGO-V_2O_5/ZnO as shown in Fig. 7b.

rGO has an absorption edge at 256 nm (Fig. 7a) which agrees with the earlier report [8]. rGO-V_2O_5/ZnO absorption spectrum is wider compared to individual rGO and V_2O_5/ZnO nanomaterials. The inclusion of rGO clearly broadens the spectrum and leads to the red shift observed in absorbance in the range of ~ 250 nm (Fig. 7a). This confirms the presence of rGO in the prepared samples. Therefore, the increased bandgap and the observed wide absorption peaks indicate that the prepared NCs could have good photovoltaic behaviour. In both NCs we can see nearly the same cut-off wavelength but with a large

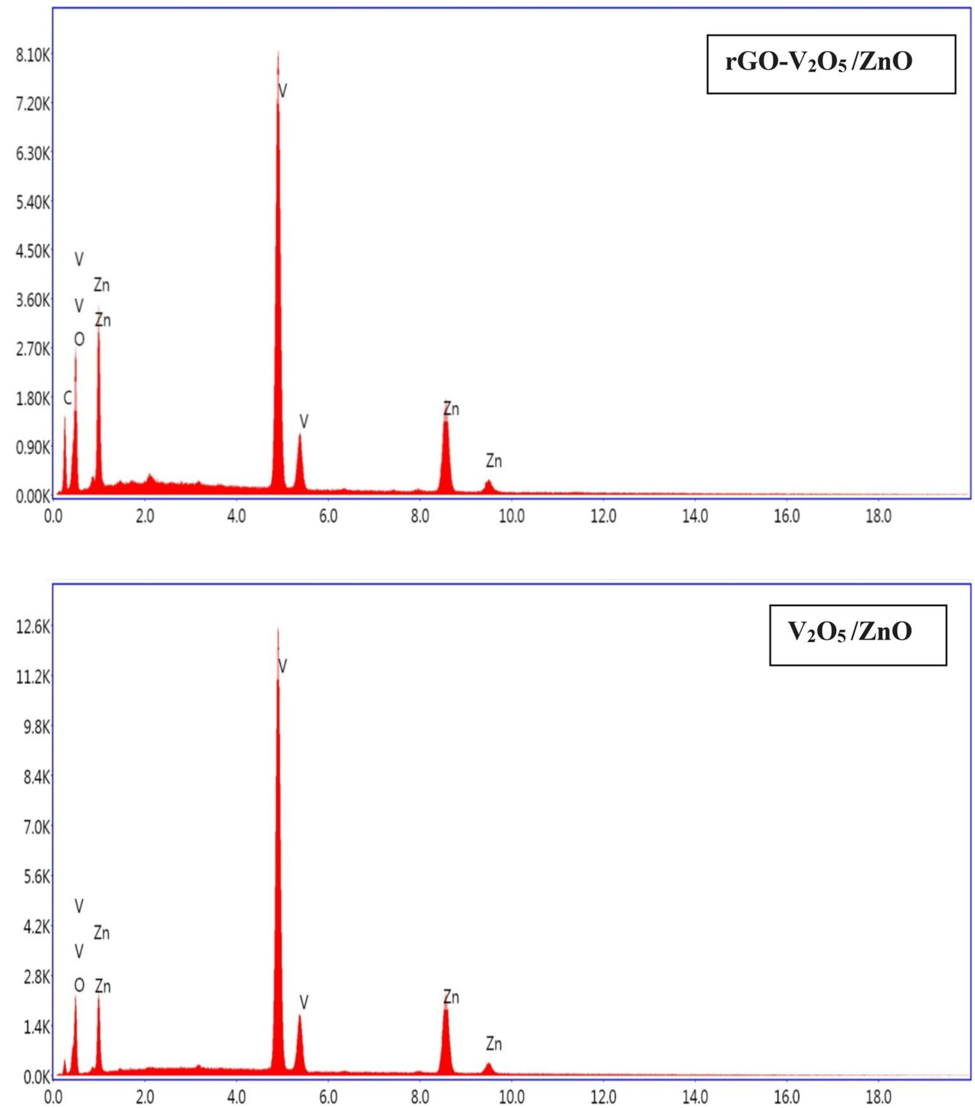

Fig. 5 EDX images of rGO-V_2O_5/ZnO and V_2O_5/ZnO nanocomposites

difference in absorption coefficient. This also shows the significant role of rGO.

3.5 FT-IR spectrum

FT-IR spectrum for rGO-V_2O_5/ZnO NCs was recorded in the range of 400–4000 cm^{-1} and is shown in Fig. 8. From the FTIR spectrum, various functional groups and metal oxide (MO) bonds present in the composite were analyzed. The vibration bands observed in the ranges from 600 to 850 cm^{-1}, which are attributed to the characteristic stretching modes of Zn–O and V=O bonds. The peaks at 622 cm^{-1} (asymmetric stretching V–O–V), 835 cm^{-1} (symmetric stretching, V–O), 1012 cm^{-1} (symmetric stretching, V=O) and the peak were observed at 516 cm^{-1} indicated Zn–O band [30]. A tiny band at 2923 cm^{-1} is due to C-H groups. A wide band at 3439 cm^{-1} indicates the presence of hydroxyl residue [31, 32].

3.6 Photoluminescence (PL) spectrum

Photoluminescence (PL) spectra of the rGO-V_2O_5/ZnO NCs are shown in Fig. 9. The two typically sharp peaks observed at ~ 469 nm and 606 nm, correspond to near band edge (NBE) emission and deep level emission (DLE), respectively. A lower intensity of PL reveals low charge recombination. Both V_2O_5/ZnO NCs and rGO-V_2O_5/ZnO NCs exhibit approximately the same wavelength (nm) range but rGO-V_2O_5/ZnO NCs shows lowest intensity compared to the other, which suggests that there is electron–hole (e–h) pair recombination in the synthesized rGO-V_2O_5/ZnO. PL studies shows good agreement with UV–Vis studies and revealed that the synthesized NCs could be used in opto-electronic devices.

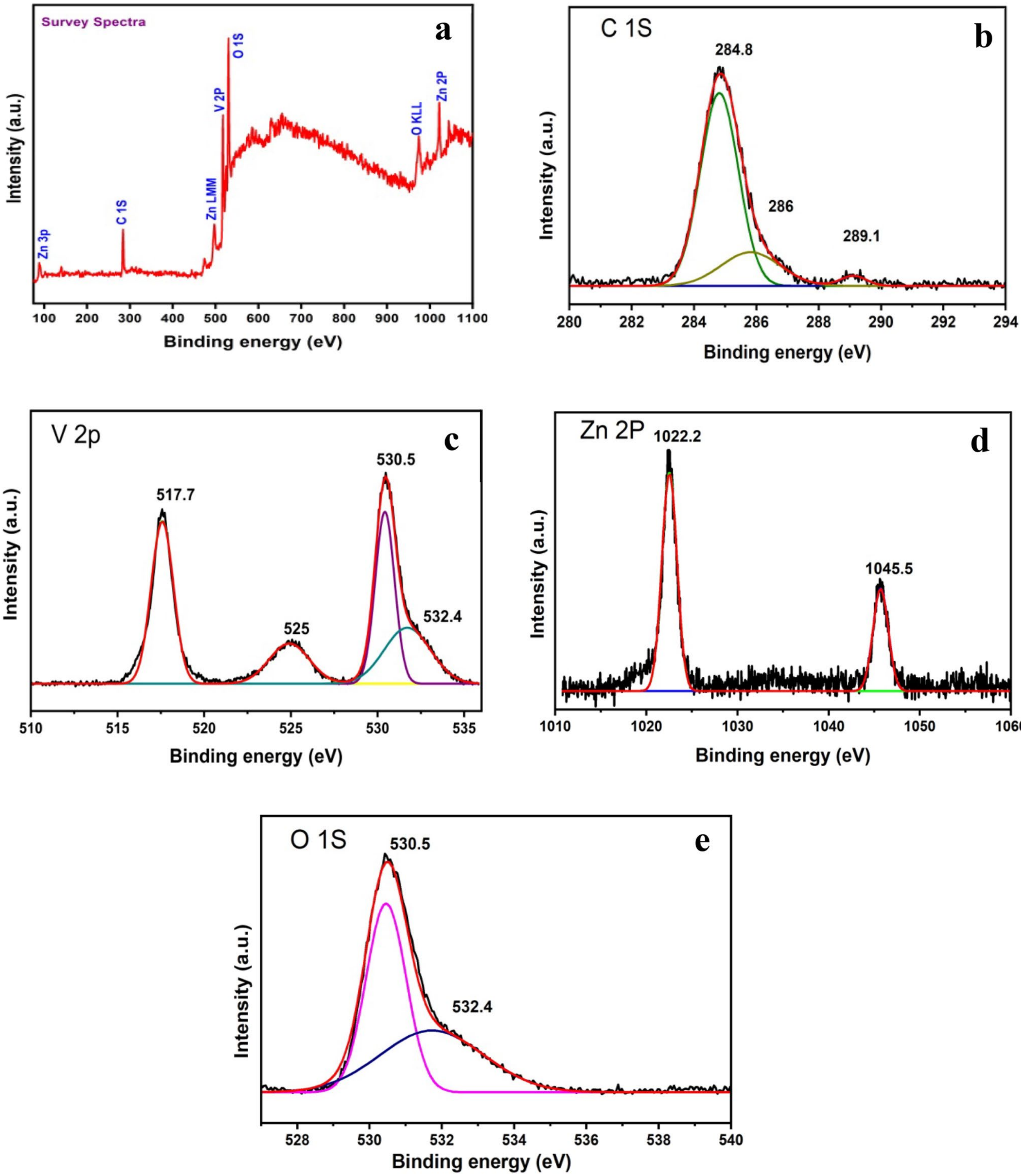

Fig. 6 **a** XPS Survey spectrum of rGO-V_2O_5/ZnO nanocomposites **b** C 1 s peaks **c** V 2p peaks **d** Zn 2p peaks **e** O 1 s peaks

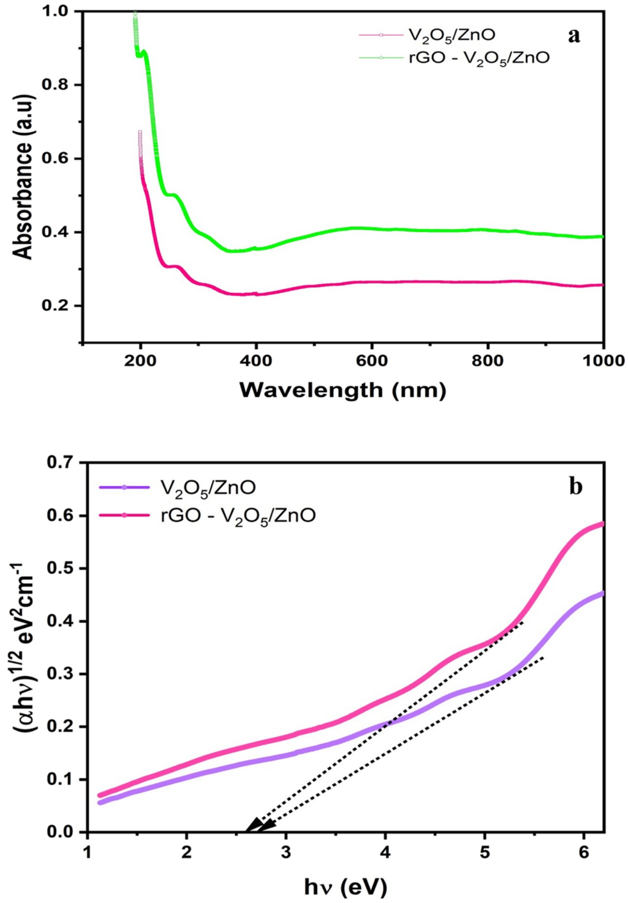

Fig. 7 UV absorption spectrum (**a**) and Tauc's plot (**b**) for prepared nanocomposites

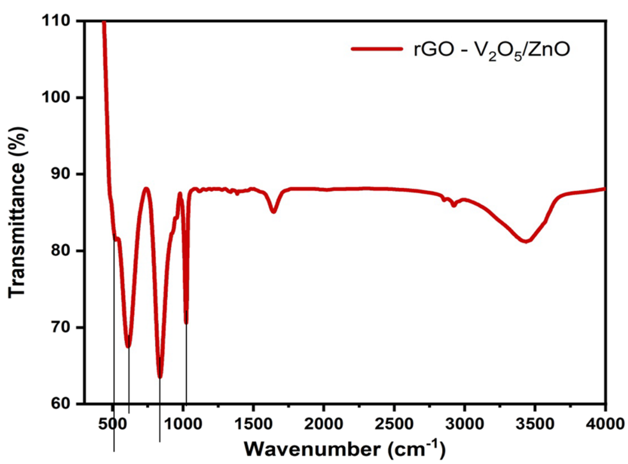

Fig. 8 FT-IR Spectrum of rGO-V_2O_5 /ZnO nanocomposites

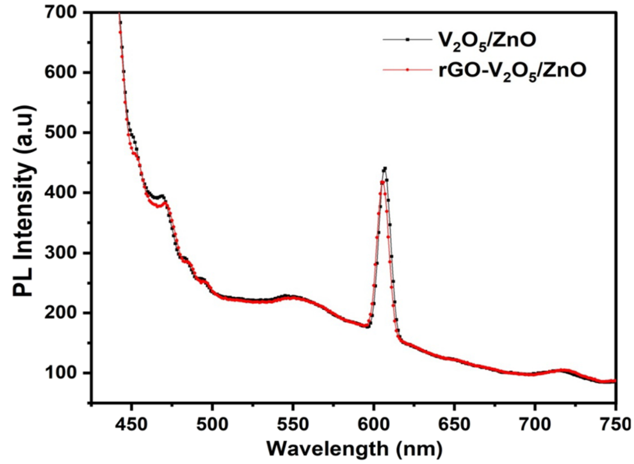

Fig. 9 Photoluminescence spectrum for prepared nanocomposites

3.7 Electrical studies

3.7.1 Hall effect analyses

The electrical properties such as carrier concentration (n), mobility (μ), resistivity (ρ) and conductivity (σ) for the synthesized rGO-V_2O_5/ZnO NCs are studied using the Hall effect method and the results are shown in Table 1. From the earlier reports [33, 34], it is clear that pure V_2O_5 and ZnO possess n-type conductivity, while in case of rGO it behaves either as p- or n-type material depending on the temperature treatment. In this work, the Hall effect results reveal that the prepared nanocomposites exhibit n-type behaviour and the carrier concentration is found to be 4.94×10^{12} cm^{-3}. Mobility is an important parameter to consider in assessing the performance of photovoltaic (PV) devices. A higher mobility will reduce the recombination of photo-generated charges and increases the efficiency of PV devices.

3.7.2 Nyquist plots

Electrochemical Impedance Spectroscopy (EIS) is used to generate Nyquist plots for investigating the charge transfer process and determining the values of resistance and capacitance of the devices. The characterization is analyzed in the frequency range of 100–400,000 Hz. Nyquist plots were drawn for real parts and imaginary parts of the impedance values in X and Y axis, respectively. The value of real impedance depicts the value of the resistance of the samples. The resistance of rGO-V_2O_5/ZnO NCs, which can be analysed from the Nyquist plots by measuring the diameter of the semicircle (Fig. 10), was found to be ~ 6500 Ω. The higher resistance value will slow down the movement of electrons in this aspect and from earlier reports we can conclude that rGO-V_2O_5/ZnO NCs have lower resistance values,

Table 1 Hall Effect measurements of rGO-V_2O_5 / ZnO NCs

Sample	Type	Hall coefficient	n (cm^{-3})	μ ($cm^2V^{-1}S^{-1}$)	ρ (Ωcm)	σ (Ω^{-1} cm^{-1})
rGO -V_2O_5/ZnO	n	1.87×10^6	4.94×10^{12}	2375	1.82×10^{-3}	4.05×10^2

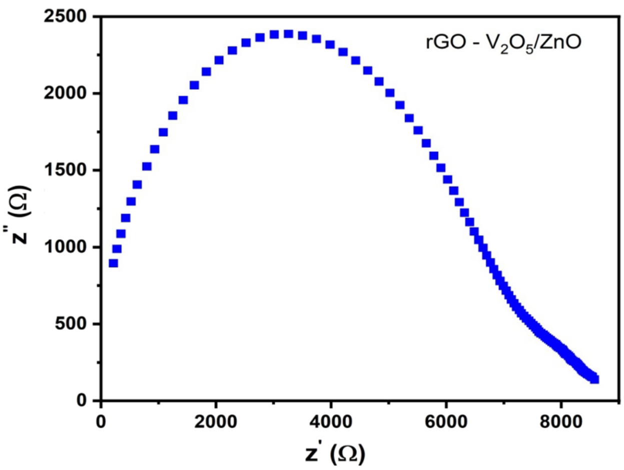

Fig. 10 Nyquist Plot of rGO-V_2O_5/ZnO nanocomposites

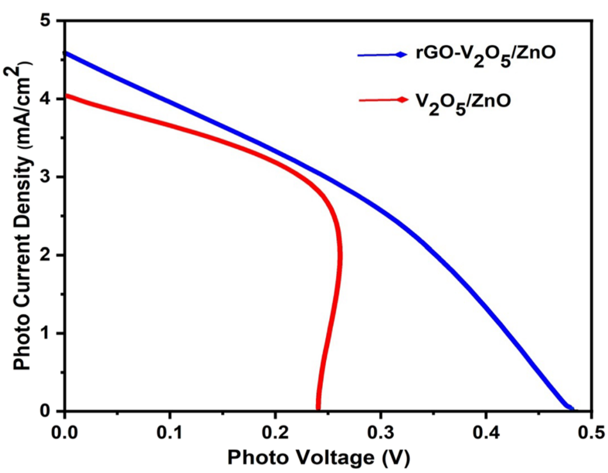

Fig. 11 J–V Characteristic curves of rGO-V_2O_5/ZnO nanocomposites photoanode based DSSCs

which are revealed from the electrical studies. This finding confirms the enhanced photovoltaic (PV) behaviour of the rGO-V_2O_5/ZnO NCs.

3.8 Photoelectrochemical (PEC) parameters

Current density–Voltage (J–V) curves of the prepared V_2O_5/ZnO and rGO-V_2O_5/ZnO photoanodes are (Fig. 11) measured under simulated 100 mW/m^2 power generation.

Table 2 Photoelectrochemical (PEC) parameters for V_2O_5/ZnO and rGO-V_2O_5/ZnO DSSCs

Sample	J_{SC} mA/cm^2	V_{OC} V	FF %	η %
V_2O_5/ZnO	4.028	0.245	0.72	0.715
rGO-V_2O_5/ZnO	4.64	0.461	0.58	1.201

The fill factor (FF) and power conversion efficiency (η) of fabricated DSSCs are estimated using the relation given by Eqs. (1) and (2).

$$FF = J_{max}.\ V_{max} / J_{sc}.\ V_{oc} \tag{1}$$

where, J_{max} is the maximum current density, V_{max} is the maximum voltage, J_{sc} is the short-circuit current, V_{oc} is the open-circuit voltage and P_{in} is the power of incident light. Power conversion efficiency (PCE) was determined using Eq. 2

$$\eta = J_{sc}.\ V_{oc}.\ F / P_{in}.100\% \tag{2}$$

From Fig. 11, it can be observed that rGO-V_2O_5/ZnO photoanodes exhibit higher device performance than V_2O_5/ZnO photoanodes. The cells based on rGO-V_2O_5 / ZnO photoanodes show an enhanced PEC values which are tabulated in Table 2. The work function of reduced graphene is sufficient for charge separation, and addition of rGO can increase the electrical conductivity of photoanodes [35, 36]. Thus, the rGO serves as the electron acceptor and facilitate rapid transport of photo generated electrons, thereby decreases the e–h recombination rates [37–40]. The lower power conversion efficiency (PEC) values for V_2O_5/ZnO photoanodes may be due to less conduction path between anodes and low dye loading behaviour. Furthermore, adding rGO enhances the efficiency of DSSCs, which can be evidently proved by electrical analysis and J–V curves. Table 3 various Photoanode materials and their photoconversion efficiencies. Though various photoanodes with higher efficiency have been reported earlier, rGO-V_2O_5/ZnO NCs as photoanodes for DSSCs have been successfully fabricated for the first time and reported in this work. DSSCs with V_2O_5/ZnO exhibit a short-circuit current density of 4.02 mA/cm^2, an open-circuit voltage of 0.245 V, fill factor of 0.72% and overall efficiency as 0.71%.

Table 3 Various photoanode materials and their photoconversion efficiencies

Photoanode material	Method	PCE (%)	References
TiO_2 aerogels	Sol gel	5.2	[38]
TiO_2 Nanoleaves	Anodization	8.5	[39]
TiO_2/ZnO	Anodization	3.98	[40]
TiO_2–CdX	Hydrothermal	13.3	[41]
Ag@C @ZnO	Hydrothermal	3.60	[42]
Ta-doped SnO_2	Spray pyrolysis	3.36	[43]
Ag-doped SnO_2/TiO_2	Hydrothermal	6.93	[44]
TiO_2 -SnO_2	hybrid sol–gel	4.96	[45]
NiS/AB (acetylene black)	Electrochemical deposition	6.75	[46]
Ni_3S_2@MWCNTs	Hydrothermal	7.48	[47]
f-MWCNTs@$NiMoSe_2$	Hydrothermal	7.39	[48]
CoS_2@MWCNT	Hydrothermal	8.85	[49]
rGO/$NiFe_2O_4$	Hydrothermal	8.41	[50]
rGO/$ZnFe_2O_4$	Hydrothermal	8.71	[51]

4 Conclusions

In summary, a solid-state reaction method was used for the synthesis of rGO-V_2O_5/ZnO and V_2O_5/ZnO NCs as photoanodes in DSSCs which were successfully fabricated and characterized. Powder XRD, SEM with EDX, XPS and FTIR results confirmed the successful formation of the NCs. Morphological analysis revealed the uniform formation of rGO-V_2O_5/ZnO and V_2O_5/ZnO NCs with average particle size around 13 ~ 25 nm and 20–60 nm, respectively. The Tauc's plots revealed a bandgap energy of 3.14 eV and provided evidence that the inclusion of rGO made the absorption spectrum wider, caused a red shift obtained in the UV–Vis absorbance, and introduced changes in the charge transfer behaviour of photovoltaic (PV) process. In addition, the incorporation of rGO in the V_2O_5/ZnO NCs improved the PCE parameters such as open-circuit voltage, short-circuit current density, FF and efficiency of fabricated DSSCs. The low resistance and carrier concentration values and high mobility nature further helped for the enhancement of the photovoltaic (PV) performances. Overall, the structural, optical and electrical results for the prepared rGO-V_2O_5/ZnO NCs indicate that high performance photovoltaic (PV) devices can be achieved.

Acknowledgements The authors would like to extend their gratitude to Tamil Nadu State Council for Science and Technology—RFRS 19-20 for the financial support of the work.

Declarations

Conflict of interest The authors declare that they have no known competing financial interests or personal relationships that could have appeared to influence the work reported in this paper.

References

1. Barnett CJ, White AO, Barron AR (2021) Size dependent conduction characteristics of catalyst-multi-walled carbon nanotube junction. Carbon Lett 31:1015–1021
2. Shaker M, Ghazvini AAS, Qureshi FR, Riahifar R (2021) A criterion combined of bulk and surface lithium storage to predict the capacity of porous carbon lithium-ion battery anodes: lithium-ion battery anode capacity prediction. Carbon Lett 31:985–990
3. Infant Shyam Kumar M, Shahil Kirupavathy S, Shalini S (2021) Exploration on reduced graphene oxide/strontium pyro niobate electrode material for electrochemical energy storage applications. Carbon Lett 31:619–633
4. Asghar F, Murtaza B, Shakoor B, Iqbal N, Shafique M, Murtaza R, Butler IS (2023) Properties, assembly and characterization of carbon nanotubes: their application in water purification, environmental pollution control and biomedicines-a comprehensive review. Carbon Lett 33:275–306
5. Medetalibeyoğlu H (2021) An investigation on development of a molecular imprinted sensor with graphitic carbon nitride (g-C_3N_4) quantum dots for detection of acetaminophen. Carbon Lett 31:1237–1248
6. Akash Prabhu S, Kavithayeni V, Suganthy R, Geetha K (2021) Graphene quantum dots synthesis and energy application: a review. Carbon Lett 31:1–12
7. Le Khac T, Kang M, Tam Tran V, Kim SW (2019) Relation of photoluminescence and sunlight photocatalytic activities of pure V_2O_5 nanohollows and V_2O_5/RGO nanocomposites. Mater Sci Semicond Process 100:159–166
8. An X, Xing G, Wang J, Tian Y, Liu Y, Wan Q (2021) Preparation of activated carbon spheres and their electrochemical properties as supercapacitor electrode. Carbon Lett 31:667–676
9. Su J, Xin Zou X, Dong Li G, Wei X, Yan C, Wang Y-N, Zhao J, Zhou L-J, Chen J-S (2011) Macroporous $V_2O_5BiVO_4$ composites: effect of heterojunction on the behavior of photogenerated charges. J Phys Chem C 115:8064–8071
10. Amano F, Tanaka T, Funabiki T (2004) Steady-state photocatalytic epoxidation of propene by O_2 over V_2O_5/SiO_2 photocatalysts. Langmuir 20:4236–4240

11. Jianhua L, Rong Y, Songmei L (2007) Synthesis and photocatalytic activity of $Ti0_2/V_2O_5$ composite catalyst doped with rare earth ions. J Rare Earths 25:173–178
12. Saravanan R, Gupta VK, Mosquera E, Gracia F (2014) Preparation and characterization of V_2O_5/ZnO nanocomposite system for photocatalytic application. J Mol Liq 198:409–412
13. Yin H, Yu K, Song C, Huang R, Zhu Z (2014) Synthesis of Au-decorated V_2O_5@ZnO heteronanostructures and enhanced plasmonic photocatalytic activity. ACS Appl Mater Interfaces 6:14851–14860
14. Wang Y, Liu L, Xu L, Cao X, Li X, Huang Y, Meng C, Wang Z, Zhu W (2014) $Ag_2O/TiO_2/V_2O_5$ one-dimensional nanoheterostructures for superior solar light photocatalytic activity. Nanoscale 6:6790
15. Boruah PK, Szunerits S, Boukherroub R, Das MR (2018) Magnetic Fe_3O_4@V_2O_5/rGO nanocomposite as a recyclable photocatalyst for dye molecules degradation under direct sunlight irradiation. Chemosphere 191:503–513
16. Aawani E, Memarian N, Dizaji HR (2019) Synthesis and characterization of reduced graphene oxide—V_2O_5 nanocomposite for enhanced photocatalytic activity under different types of irradiation. J Phys Chem Solids 125:8–15
17. Farahmandjou M, Abaeiyan N (2017) Chemical synthesis of vanadium oxide (V_2O_5) nanoparticles prepared by sodium metavanadate. J Nanomed Res 5(1):00103
18. Li P, Ma X, Liang Y, Tan J, Wang L (2019) Preparation and electrochemical capacitive properties of C-MnO_2 composite with foam-like structure based on modified rubber. Carbon Lett 29:547–552
19. Seok S, Jang D, Kim H, Park S (2020) Production of NiO/N-doped carbon hybrid and its electrocatalytic performance for oxygen evolution reactions. Carbon Lett 30:485–491
20. Ma Y, Liu Y (2022) Preparation of graphene-ZnO composite with enhanced photocatalytic performance. Carbon Lett 32:1265–1275
21. Sasikumar R, Chena T-W, Chena S-M, Rweib S-P, Ramaraj SK (2018) Developing the photovoltaic performance of dye-sensitized solar cells (DSSCs) using a SnO_2-doped graphene oxide hybrid nanocomposite as a photo-anode. Optical Mater 79:348–352
22. Ranganathan P, Sasikumar R, Chen S-M, Rwei S-P, Sireesha P (2017) Enhanced photovoltaic performance of dye-sensitized solar cells based on nickel oxide supported on nitrogen-doped graphene nanocomposite as a photoanode. J Colloid Interface Sci 504:570–578
23. Sireesha P, Sasikumar R, Chen S-M, Su C, Ranganathan P, Rwei S-P (2017) Carboxylic acid-functionalized multi-walled carbon nanotubes-polyindole/Ti_2O_3, a novel hybrid nanocomposite as highly efficient photo-anode for dye-sensitized solar cells (DSSCs). Appl Surface Sci 423:147–153
24. Murugadoss V, Wang N, Tadakamalla S (2017) In-situ grown cobalt selenide/graphene nanocomposites counter electrode for enhanced dye-sensitized solar cell performance. J Mater Chem A 5:14583–14594
25. Stobinski L, Lesiak B, Malolepszy A, Mazurkiewicz M, Mierzwa B, Zemek J, Jiricek P, Bieloshapka I (2014) Graphene oxide and reduced graphene oxide studied by the XRD, TEM and electron spectroscopy methods. J Electron Spectrosc Relat Phenom 195:145–154
26. Azarang M, Shuhaimi A, Sookhakian M (2015) Crystalline quality assessment, photocurrent response and optical properties of reduced graphene oxide uniformly decorated zinc oxide nanoparticles based on the graphene oxide concentration. RSC Adv 5:53117
27. Venkateshalu S, Cherusseri J, Karnan M, Kumar KS (2020) New method for the synthesis of 2D vanadium nitride (MXene) and its application as a supercapacitor electrode. ACS Omega 5(29):17983–17992
28. Bhagya Lakshmi C, Jayalakshmi S, Annavenus S (2021) Exploring CuBiSe/Y_2O_3 nanocomposite material as a working electrode in photoelectrochemical cell. J Xi'an Shiyou Univ Nat Sci 17:305–316
29. Wongrerkdee S, Moungsrijun S (2021) Linking bridge improvement of ZnO/N719 interfaces via ammonia treatment for efficiency enhancement of dye-sensitized solar cell. Surf Interfaces 23:100991
30. Shukla P, Shukla JK (2018) Facile sol-gel synthesis and enhanced photocatalytic activity of the V_2O_5-ZnO nanoflakes. J Sci 3:452–455
31. Rana SSTKGD, Mukut IRABGS, Chattopadhyay CD (2016) Studies on synthesis of reduced graphene oxide (RGO) via green route and its electrical property. Mater Res Bull 79:41–51
32. Nagaraju G, Udayabhanu, Shivaraj, Prashanthb SA, Shastri M, Yathish KV, Anupama C, Rangappa D (2017) Electrochemical heavy metal detection, photocatalytic, photoluminescence, biodiesel production and antibacterial activities of Ag-ZnO nanomaterial. Mater Res Bull 94:54–63
33. Ragupathi V, Babu MM, Panigrahi P, Ganapathi Subramaniam N (2020) Enhanced electrical and optical properties of Al doped and ZnO nanoparticles for optoelectronic application: ecofriendly green route. IOP Publish J Phys 1495:012040
34. Tu NDK, Choi J, Park CR, Kim H (2015) Remarkable conversion between n- and p-type reduced graphene oxide on varying the thermal annealing temperature. Chem Mater 27:7362–7369
35. Tang Y-B, Lee C-S, Xu J, Liu ZT, Chen Z, He Z, Cao YL, Yuan G, Song H, Chen L (2010) Incorporation of graphenes in nanostructured TiO_2 films via molecular grafting for dye-sensitized solar cell application. ACS Nano 4:3482–3488
36. Yang N, Zhai J, Wang D, Chen Y, Jiang L (2010) Two-dimensional graphene bridges enhanced photoinduced charge transport in dye-sensitized solar cells. ACS Nano 4:887–894
37. Wiatrowski A, Mazur M, Obstarczyk A, Wojcieszak D (2018) Comparison of the physicochemical properties of TiO_2 thin films obtained by magnetron sputtering with continuous and pulsed gas flow. Coatings 8:412
38. Alwin S, Shajan XS, Karuppasamy K, Warrier KGK (2017) Microwave assisted synthesis of high surface area TiO_2 aerogels: a competent photoanode material for quasi-solid dye-sensitized solar cells. Mater Chem Phys 196:37–44
39. Deepak TG, Anjusree GS, Pai KRN, Subash D, Nair Sv, Nair AS (2014) Cabbage leaf-shaped two-dimensional TiO_2 mesostructures for efficient dye-sensitized solar cells. RSC Adv 4(51):27084–27090
40. Ren J, Que W, Yin X, He Y, Javed HMA (2014) Novel fabrication of TiO_2/ZnO nanotube array heterojunction for dye-sensitized solar cells. RSC Adv 4(15):7454–7460
41. Bhattacharya S, Datta J (2020) Wide-low energy coupled semiconductor layers of TiO_2–CdX boosting the performance of DSSC. Sol Energy 208:674–687
42. Ansir R, Ullah N, Ünlü B, Mujtaba Shah S, Özacar M (2021) Effect of annealing temperatures on performance of DSSCs fabricated using Ag or Pd@C@ZnO composites as photoanode materials. Sol Energy 224:617–628
43. Ramarajan R, Purushothamreddy N, Dileep RK, Kovendhan M, Veerappan G, Thangaraju K, Paul Joseph D (2020) Large-area spray deposited Ta-doped SnO_2 thin film electrode for DSSC application. Sol Energy 211:547–559
44. Khojasteh F, Mersagh MR, Hashemipour H (2022) The influences of Ni, Ag-doped TiO_2 and SnO_2, Ag-doped SnO_2/TiO_2 nanocomposites on recombination reduction in dye synthesized solar cells. J Alloys Compd 890:161709
45. Smok W, Tański T, Drygała A, Podwórny J (2022) Facile route to prepare hybrid TiO_2-SnO_2 DSSCs. Appl Surf Sci 605:154850

46. Theerthagiri J, Senthil RA, Arunachalam P, Bhabu KA, Selvi A, Madhavan J, Murugan K, Arof AK (2016) Electrochemical deposition of carbon materials incorporated nickel sulfide composite as counter electrode for dye-sensitized solar cells. Ionics 23(4):1017–1025
47. Maiaugree W, Tansoonton T, Amornkitbamrung V, Swatsitang E (2019) Ni_3S_2@MWCNTs films for effective counter electrodes of dye-sensitized solar cells. Curr Appl Phys 19(12):1355–1361
48. Mirzaei M, Gholivand MB (2021) Introduction of Pt-free counter electrode based on f-MWCNTs@$NiMoSe_2$ nanocomposite for efficient dye-sensitized solar cells. Sol Energy 227:67–77
49. Ibrahim AS, Anbarasu P, Mahendran R, Rajendran K, Sekhar KC, Sathish S (2022) Facile synthesis of cobalt sulfide/carbon nanotube composites as a low-cost Pt-free counter electrode for dye-sensitized solar cells (DSSCs). Diam Relat Mater 130:109440
50. Anto Feradrick Samson V, Bharathi Bernadsha S, Fennyl Britto J, Victor Antony Raj M, Madhavan J (2022) Synthesis of rGO/$NiFe_2O_4$ nanocomposite as an alternative counter electrode material to fabricate Pt-free efficient dye sensitized solar cells. Diam Relat Mater 130:109406
51. Samson VAF, Bernadsha SB, Paul Winston AJP, Divya D, Abraham J, Raj MVA, Madhavan J (2022) rGO sheets/$ZnFe_2O_4$ nanocomposities as an efficient electro catalyst material for I3−/I− Reaction for high performance DSSCs. J Inorg Organomet Polym Mater 32(3):1183–1189

Publisher's Note Springer Nature remains neutral with regard to jurisdictional claims in published maps and institutional affiliations.